Absolute single-photoionization cross sections of Se^{2+}: Experiment and theory

D. A. Macaluso, A. Aguilar, A. L. D. Kilcoyne, E. C. Red, R. C. Bilodeau, R. A. Phaneuf, N. C. Sterling, and B. M. McLaughlin

Phys. Rev. A **92**, 063424 — Published 28 December 2015

DOI: 10.1103/PhysRevA.92.063424

Absolute single photoionization cross-sections of Se^{2+}: Experiment and theory

D. A. Macaluso*
Department of Physics and Astronomy, University of Montana, Missoula, MT 59812

A. Aguilar,† A. L. D. Kilcoyne, and E. C. Red‡
The Advanced Light Source, Lawrence Berkeley National Laboratory, Berkeley, CA 94720

R. C. Bilodeau§
Department of Physics, Western Michigan University, Kalamazoo, MI 49008-5252 and
The Advanced Light Source, Lawrence Berkeley National Laboratory, Berkeley, CA 94720

R. A. Phaneuf
Department of Physics, University of Nevada, Reno, NV 89557-0220

N. C. Sterling
Department of Physics, University of West Georgia, Carrollton, GA 30118

B. M. McLaughlin¶
Centre for Theoretical Atomic, Molecular and Optical Physics (CTAMOP), School of Mathematics and Physics, The David Bates Building, 7 College Park, Queen's University of Belfast, Belfast BT7 1NN, United Kingdom and
Institute for Theoretical Atomic and Molecular Physics (ITAMP), Harvard Smithsonian Center for Astrophysics, 60 Garden Street, MS-14, Cambridge, MA 02138

Absolute single photoionization cross section measurements for Se^{2+} ions were performed at the Advanced Light Source (ALS) at Lawrence Berkeley National Laboratory using the merged-beams photo-ion technique. Measurements were made at a photon energy resolution of 24 ± 3 meV in the photon energy range 23.5 – 42.5 eV spanning the ground state and low-lying metastable state ionization thresholds. To clearly resolve the resonant structure near the ground state threshold, high-resolution measurements were made from 30.0 – 31.9 eV at a photon energy resolution of 6.7 ± 0.7 meV. Numerous resonance features observed in the experimental spectra are assigned and their energies and quantum defects tabulated. The high-resolution cross-section measurements are compared with large-scale, state-of-the-art theoretical cross-section calculations obtained from the Dirac-Coulomb *R*-matrix method. Suitable agreement is obtained over the entire photon energy range investigated. These results are the first experimental determination of the absolute photoionization cross section of doubly-ionized selenium and include the first detailed analysis of the photoionization resonance spectrum of this ion.

PACS numbers: 32.80.Fb, 32.80.Aa, 32.70.Cs, 95.30.Dr

I. INTRODUCTION

In spite of its cosmic rarity, atomic selenium has been detected in the spectra of stars [1, 2] and of astrophysical nebulae [3–5]. The chemical composition of these objects illuminate details of stellar nucleosynthesis and the chemical evolution of galaxies. To derive accurate elemental abundances, astronomers must account for the unobserved ionization stages of an element in nebulae, and for non-local thermodynamic equilibrium (NLTE) effects in stellar atmospheres. Both nebular and stellar NLTE abundance analyses are strongly reliant on accurate atomic data including photoionization cross sections. For example, it has been shown that atomic data uncertainties alone can result in abundance errors for neutron-capture elements (atomic number Z>30) of a factor of two or more in astrophysical nebulae [6, 7].

However, atomic data such as photoionization cross sections are unknown for the vast majority of trans-iron (or *trans-Fe*), neutron-capture element ions. To address this, the present program was instituted to measure high-energy-resolution absolute photoionization cross sections for several of the *n*-capture elements recently detected. The initial measurements of this program [8–11] have provided critically needed benchmarks to observational astronomers [7, 12, 13], confirmed results for atomic photoionization cross section calculations from a recently de-

* david.macaluso@umontana.edu
† Present address: ReVera Incorporated, 3090 Oakmead Village Drive, Santa Clara, CA 95051, USA
‡ Present address: Department of Physics, Morehouse College, Atlanta, GA 30314
§ Present address: Department of Physics, University of Connecticut, Storrs, CT 06269, USA
¶ bmclaughlin899@btinternet.com

veloped suite of fully relativistic parallel Dirac Atomic R-matrix (DARC) codes [14–19], and updated tabulated thresholds and excited-state energy levels published in the NIST atomic spectra database [10, 11, 20].

In this report we present the first experimental determination of the absolute single photoionization cross-section of Se^{2+}. These measurements were performed using merged-beam photo-ion spectroscopy at a photon energy resolution of 24 ± 3 meV in the photon energy range 23.5 eV to 42.5 eV. This energy range encompasses the ionization thresholds of the $^3P_0$ ground state and three lowest lying metastable states, the $^3P_1$, $^3P_2$, and $^1D_2$ states. Additional measurements were performed at an energy resolution of 6.7 ± 0.7 meV in the photon energy range 30.0 eV to 31.9 eV to better resolve the complex structure in the direct ionization threshold region. Analysis of the resonance structure produced three distinct Rydberg resonance series identifications with two of the three series originating from multiple initial states of Se^{2+}.

The layout of this paper is as follows. In Section II we give a brief outline of the experimental approach used to determine the absolute photoionization cross sections. Section III presents our experimental results. In Section IV DARC theoretical results are presented and in Section V the ALS experimental results are compared with these theoretical results. In Section VI conclusions and a summary of our work are presented.

II. EXPERIMENT

The measurements were conducted at the Advanced Light Source (ALS) synchrotron radiation facility at Lawrence Berkeley National Laboratory using the ion-photon-beam (IPB) end station installed at undulator Beamline 10.0.1.2 [9–11, 21–29].

In merged-beam photo-ion spectroscopy, a mass-to-charge-selected beam of ions is merged with a counter-propagating beam of monochromatized synchrotron radiation to detrermine precision atomic and molecular photoionization spectra [30]. To produce the ion beam, solid Se pellets were vaporized in a resistively-heated oven inside a 10 GHz electron-cyclotron-resonance (ECR) ion source [31, 32] and accelerated out of the ion source via a 6 kV extraction potential. The mass-to-charge of the desired ion species was selected with a 60° dipole magnet, forming the homogeneous Se^{2+} primary ion beam that was then merged with the counter-propagating photon beam. The photo-ions produced along the ∼1.4 m merged beam path were deflected and separated from the primary ion beam with a 45° dipole demerging magnet toward a set of 90° spherical-section electrostatic deflectors that directed the product ions onto a negatively-charged stainless steel plate. The impact of product ions on this plate produced secondary electrons that were accelerated onto a single-particle channeltron detector [33]. In order to separate the photo-ions from various sources of background noise, the photon beam was mechanically chopped at a frequency of 6 Hz so that background and signal+background could be alternately measured in real time. The primary ions were directed to a Faraday cup used to monitor the primary ion beam current. The 12 keV Se^{2+} primary ion beam current was typically in the 40 nA range.

For spectroscopic measurements, photo-ions produced along the entirety of the merged-beam path were selected by the demerging magnet. The photo-ion yield was measured as a function of energy by sweeping the photon energy in discrete steps ($\Delta E = 10$ meV for low-resolution measurements and 2 meV for high-resolution measurements). Absolute photoionization cross sections were measured at discrete energies which were used during data analysis to place the relative spectroscopic measurements on an absolute cross-section scale. For these measurements a potential of 1.0 kV was applied to the interaction region, which is an electrically-isolated, stainless-steel mesh cylinder 29.4 ± 0.56 cm long. This energy-tagged the photo-ions produced within the volume of the interaction region, and the demerging magnet setting was tuned so that only those photo-ions were directed to the detector. The overlap of the ion and photon beams was measured immediately before and after each absolute cross-section measurement using three translating slit scanners to accurately quantify the volume within which the tagged photo-ions were produced. Uncertainties in the absolute measurements are calculated as a quadrature sum of the individual uncertainties that arise from the characterization of the ion and photon beams and their spatial overlap, and the physical and statistical collection of photo-ions. This total uncertainty is typically 15 - 17% and is thus conservatively estimated to be 20% in the present analysis [22].

Photons were produced by electrons accelerated within a 10-cm period, 43 period undulator housed within the 1.9 GeV, 400 mA (at the time) constant-current storage ring of the ALS. Downstream of the undulator, a spherical-grating monochromator with three interchangeable diffraction gratings was used to select the particular photon energy and energy resolution of the collimated photon beam. The photon flux was monitored with a silicon photodiode (IRD, SXUV-100) referenced to a second photodiode from the same manufacturing batch that was absolutely calibrated by both NIST and the PTB at BESSY II in different photon energy ranges.

The contribution to the total photoionization cross section due to the production and transmission of higher-order radiation from the undulator and monochromator at Beamline 10 must be addressed [34]. While second-order radiation is primarily off-axis and can be largely reduced by the use of lateral baffles, third-order radiation is well collimated and collinear with the first-order output. Third-order radiation is therefore present in the photon beam at all energies and can represent a significant fraction of the total photon flux. However, a detailed analysis of the higher-order light production of the undulator and

monochromator at beamline 10.0.1.2 was recently published [10] which demonstrated that third-order photons represent a significant fraction of the photon beam only at the lowest energies of the low-energy grating (i.e., below 20 eV). By 30 eV, third-order photons were shown to represent less than 5 percent of the photons exiting the monochromator, and by 40 eV this percentage is below 1 percent. This indicates the measured structure in the energy range below the $^1D_2$ threshold at ∼30 eV is predominantly due to first-order radiation. To verify this, spectroscopic measurements were conducted at three-times the photon energy range to look for similar structures at their first-order energies. No such structures were found, so the contribution to the measured photoionization signal due to the presence of higher-order photons can be neglected in these measurements.

The photon energy scale for these measurements was calibrated using the doubly-excited autoionizing states of He [35] in first, second, and third order on a side-branch gas cell. These calibrations produced an energy uncertainty conservatively estimated to be ± 10 meV, which is typical for such measurements at beamline 10.0.1.2. In addition, the spectra were measured on multiple beamtimes distributed over several years with energy calibrations that agree to well within the quoted energy uncertainty.

III. EXPERIMENTAL RESULTS AND ANALYSIS

A. 24 meV Photon Energy Resolution Measurements

The $^{78}Se^{2+}$ absolute single photoionization cross section spectrum measured at 24 meV photon energy resolution was constructed from 20 individual scans with a minimum of 0.3 eV overlap between adjacent scans (Figure 1). The solid circles with error bars correspond to the 11 absolute cross-section measurements (Table I) that were used to place the relative photo-ion yield spectrum on an absolute scale.

To facilitate the tabulated identifications of each Rydberg series of resonances, all features are numbered as indicated in Figure 2. In instances where features are composed of multiple resonances and the individual resonances are only partially-resolved, a lettering subdesignation is used. In instances where no clear distinction can be made between individual features, a single identification number is used instead and thus the same feature number may appear in multiple series. In the case of the prominent features just above the $^3P_1$, $^3P_2$, and $^1D_2$ metastable state thresholds, the designation *High Resolution Group* was added (HR Group 20, 21, and 22 in Figure 2). These features were subsequently measured at higher energy resolution and are analyzed in the following section. The NIST Atomic Spectra Database [20] was the primary source for the energy levels used in the Rydberg series analysis (Table II and Table III). The Cowan atomic structure code available online from Los Alamos National Laboratory [36] was also used during this stage of analysis. While the Cowan code typically cannot be used to reliably determine absolute feature energies, it is an expedient method for calculating approximate energy differences (between initial and intermediate excited states, for example), and thus it was a valuable tool during resonance series identifications. The Cowan code was also used to identify the

TABLE I. Se^{2+} absolute single photoionization valence shell cross-section measurements made at the ALS with a 24 ± 3 meV photon energy resolution in the photon energy range 25 – 42 eV.

Energy (eV)	σ (Mb)
25.800	0.10 ± 0.02
27.500	0.14 ± 0.03
29.200	0.13 ± 0.03
31.000	0.30 ± 0.06
31.257	1.27 ± 0.25
31.784	1.08 ± 0.22
34.485	1.39 ± 0.28
35.000	0.66 ± 0.13
37.150	0.56 ± 0.11
39.132	1.48 ± 0.30
42.000	0.49 ± 0.10

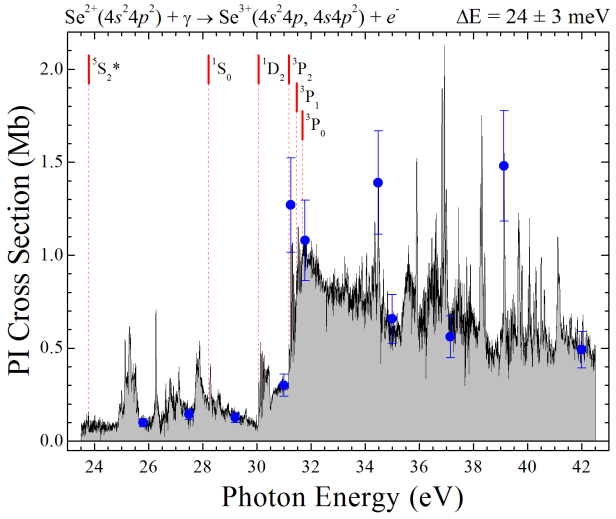

FIG. 1. (Color online) Absolute $Se^{2+} \rightarrow Se^{3+}$ photoionization cross section measured at 24 ± 3 meV photon energy resolution. Solid blue circles with error bars represent absolute cross-section measurements used to place the relative photo-ion yield spectrum on an absolute scale (Table I). The $^3P_0$ ground state and $^3P_1$, $^3P_2$, $^1D_2$, and $^1S_0$ metastable state ionization thresholds are indicated by vertical bars with dashed lines [20]. The $^5S_2^o$ metastable state ionization threshold is indicated as predicted by the Cowan atomic structure code [36]

TABLE II. Energy levels of Se^{2+} from the NIST tabulations [20] and those examined in the present analysis.

Configuration	Term	J	NIST (eV)	Expt./Theory (eV)
$3d^{10}4s^24p^2$	^3P	0	0.000	0.000 ± 0.000
		1	0.216	0.216 ± 0.010
		2	0.488	0.490 ± 0.010
$3d^{10}4s^24p^2$	^1D	2	1.616	1.614 ± 0.010
$3d^{10}4s^24p^2$	^1S	0	3.525	3.735 ± 0.236[a]
$3d^{10}4s4p^3$	$^5S^o$	2	–	8.015 ± 0.150[a]
				7.890 ± 0.150[b]

[a]Closed channel DARC calculations.
[b]Estimated from the Cowan code [36].

TABLE III. Energy levels of Se^{3+} from the NIST tabulations [20] and those examined in the present analysis.

Configuration	Term	J	NIST (eV)	Expt./Theory (eV)
$3d^{10}4s^24p$	$^2P^o$	1/2	0.000	0.000 ± 0.000
		3/2	0.543	0.552 ± 0.010
$3d^{10}4s4p^2$	^4P	1/2	9.844	9.834 ± 0.010
		3/2	10.040	10.030 ± 0 .010
		5/2	10.360	9.705 ± 0.140[a]
$3sd^{10}4s4p^2$	^2D	3/2	12.921	13.059 ± 0.140[a]
		5/2	12.982	12.960 ± 0.010

[a]GRASP calculations.

$^1P_1$ and $^1S_0$ intermediate-state, fine-structure coupling terms in Table V and Figure 3. Our ionization potential values were also compared with large-scale DARC closed channels calculations.

To assign transitions to the observed resonance structure, the quantum defect form of the Rydberg equation [37] was used,

$$E_n = E_\infty - \frac{(Z - N_c)^2}{(n - \delta_n)^2} \quad (1)$$

where E_n is the resonance energy, E_∞ is the series limit (where $n = \infty$), Z is the nuclear charge, N_c is the number of core electrons, n is the principal quantum number of the associated resonance, and δ is the quantum defect parameter. This parameter quantifies the deviation from a purely hydrogenic model due to incomplete screening of the nucleus as a result of core penetration by the active electron. Typically, δ values are between 0 and 1 where values greater than 1 may indicate an incorrect principal quantum number assignment for a particular

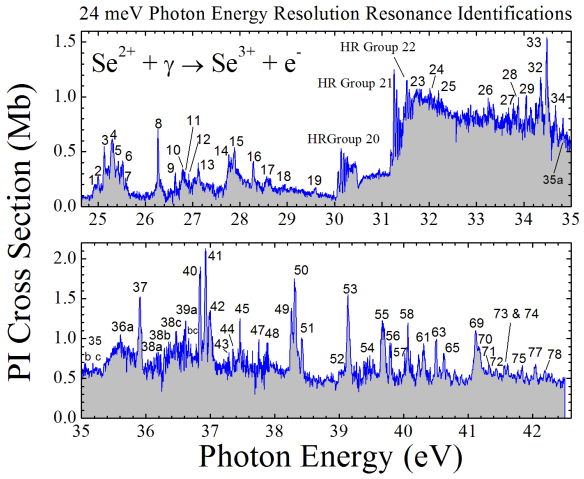

FIG. 2. (Color online) Resonance feature numbering scheme used in the Se^{2+} Rydberg series identification tables associated with the 24 meV photon energy resolution spectrum.

resonance or resonance series. Quantum defect values were free parameters in the present analysis; however, they were constrained to remain between 0 and 1 and be approximately constant for a given series identification.

As seen in the Rydberg formula, δ values are a function of n and the excitation energy of each resonance for a given series assignment so the uncertainty in δ is related to the energy uncertainty and resolution of these measurements. In cases where multiple peaks coincide, the ability to distinguish individual resonances also affects the determination of δ values. In addition, the δ parameter has decreasing influence on the calculated resonance energy as the quantum number increases so each δ has its own unique uncertainty. Due to the complexity of these relations, error bars for δ have been omitted and the presented δ values can be considered accurate to within the quoted energy uncertainty and resolution of these measurements.

For the 24 meV energy resolution analysis, the series limits and ionization potential were initially set using the values reported by NIST. However, initial identifications were impossible as the ionization potential of Se^{2+}, reported at the time to be 30.8204 eV, was in clear disagreement with measurements. This motivated additional high-resolution measurements that were subsequently used to determined the actual IP to be 31.685 eV ± 10 meV (the details of this discrepancy and the determination of the IP are included in Section III.B). After the IP was corrected, the Rydberg series identifications progressed as usual by starting with the NIST-tabulated values for the initial states of Se^{2+} and the final states of Se^{3+}. Once rough series identifications were made, the initial and final states were allowed to be free parameters within the constraint of maintaining approximately constant δ-values for a given series. The n-values of the

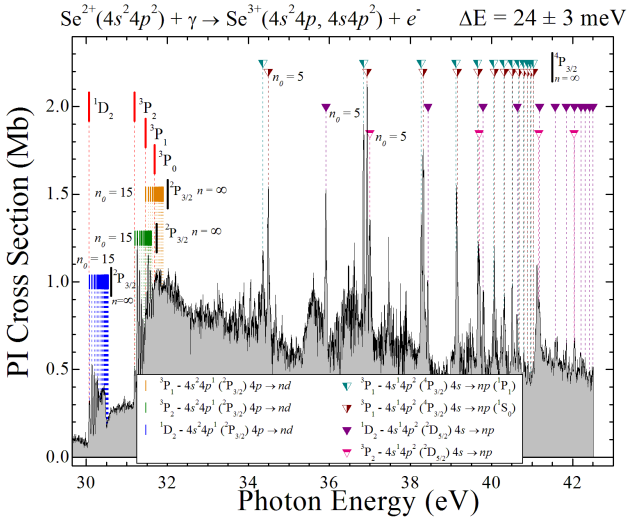

FIG. 3. (Color online) Rydberg series of resonances due to $4s \rightarrow np$ and $4p \rightarrow nd$ transitions converging to the $4s^2 4p$ ($^2P_{3/2}$) and $4s4p^2$ ($^4P_{3/2}$, $^2D_{5/2}$) series limits in Se^{3+}. Series limits are indicated by heavy vertical bars with corresponding labels. The ionization thresholds for the $^3P_0$ ground state and $^3P_1$, $^3P_2$, and $^1D_2$ metastable states are indicated by vertical bars with dashed lines [20]. The series limits for the series converging to the $^2D_{5/2}$ state in Se^{3+} are beyond the energy scale of the plot and are not included in the figure.

initial resonances of each series were determined using quantum defect thoery and were verified using the Cowan code [36]. In all but one case, the present analysis is in agreement with the NIST-reported values to within the energy uncertainty of these measurements (Table II and Table III). The lone exception is the $^2D_{5/2}$ level of Se^{3+} as seen in Table III which was found to be 22 meV below the NIST-reported value.

Two distinct Rydberg resonance series have been identified in the 24 meV energy-resolution spectrum (Figure 3). These series are due to $4s \rightarrow np$ autoionizing transitions originating from the $^3P_1$, $^3P_2$, and $^1D_2$ metastable states of Se^{2+} ($n_o = 5$ in each case, where n_o is the principal quantum number of the first detected member of the series). The series converging to the $^2D_{5/2}$ limit in Se^{3+} is seen originating from both the $^1D_2$ and $^3P_2$ metastable states of Se^{2+} as indicated by solid triangles and top-half-filled triangles, respectively, in Figure 3. The details of this series are listed in Table IV. A second identified series converges to the $^4P_{3/2}$ series limit and is seen originating from the $^3P_1$ metastable state (left and right half-filled triangles, Figure 3). This series is unique in that fine-structure splitting of the intermediate excited states is apparent with splitting of the first three members clearly resolved (feature numbers 32/33, 40/41, and 49/50). The remaining higher-energy resonances of the split series are no longer resolved and thus share feature identification numbers above 50. The details of this series are listed in Table V. An additional series is seen occuring directly above the thresholds of the same three metastable states and converging to the $^2P_{3/2}$ series limit in Se^{3+}. However, this series was identified in the 6.7 meV energy-resolution spectrum so the detailed description and analysis of this series is in the following section and it is included here only for comparison.

B. 6.7 meV Photon Energy Resolution Measurements

Initial attempts to assign transitions to certain Rydberg series in the 24 meV-energy-resolution spectrum failed (HR Groups 20, 21, and 22 in Figure 2). This failure was partially due to the inadequate resolution of the measurements, but initial analysis also indicated an apparent (and significant) disagreement between the reported and measured ionization potential of Se^{2+}. The region containing these features (30.0 eV to 31.9 eV) was therefore remeasured at a photon energy resolution of 6.7 ± 0.7 meV to fully resolve the individual resonances and address the apparent ionization potential discrepancy. The resulting spectrum (Figure 4) is a composite of three energy scans, each of which was measured on multiple beamtimes with separate gas-cell energy calibrations. No absolute cross-section measurements were performed for the high-resolution spectrum; instead, the integrated oscillator strength of the 24 meV energy-resolution spectrum was used to place this high-resolution spectrum on an absolute cross-section scale. To do so, the high-resolution spectrum was scaled until its integrated oscillator strength matched that of the low-resolution absolute photoionization spectrum from 30.0 eV to 31.9 eV. The final results of which are shown in Figure 5 where the additional resolving power of the high-resolution measurements is clearly evident. As an indication of the relative precision of the photon energy calibration technique, the two spectra were nearly aligned upon initial comparison, with an average discrepancy between the centroids of common features of just under 2 meV (or well below the quoted energy uncertainty of the present measurements). Because the energy calibrations of neither spectrum were prefered, this discrepancy was remedied by shifting the low-resolution spectrum up 1 meV and the high-resolution spectrum down 1 meV which produced the alignment seen in the figure.

To again facilitate the tabulated identifications of each Rydberg series of resonances, all features are numbered as indicated in Figure 6. However, the procedure for identifying these series was unusual because the ionization potential had to be left as a free parameter due to the obvious disagreement between the reported value and experiment. Initially, the ionization potential was adjusted so that the thresholds for each metastable state in the spectrum fell just below the first resonance of their associated series. This is an example of the power of high-resolution photoionization spectroscopy in combination

TABLE IV. Rydberg series of resonances due to $4s \rightarrow np$ transitions from the $^3P_2$ and $^1D_2$ metastable states of Se^{2+} converging to the $^2D_{5/2}$ series limit in Se^{3+} as identified in the 24 meV photon energy resolution spectrum. Tabulated feature numbers correspond to those identified in Figure 2.

Initial Se^{2+} states: $4s^24p^2$ ($^3P_2$, $^1D_2$)							
Rydberg Series $4s4p^2(^3P_2)$, $4s \rightarrow np$				Rydberg Series $4s4p^2(^1D_2)$, $4s \rightarrow np$			
n	Energy (eV)	δ	Feature #	n	Energy (eV)	δ	Feature #
5	34.361	0.858	32	5	34.491	0.820	33
6	36.850	0.868	40	6	36.927	0.825	41
7	38.260	0.852	49	7	38.308	0.805	50
8	39.125	0.818	53	8	39.150	0.780	53
9	39.652	0.858	55	9	39.667	0.820	55
10	40.055	0.790	58	10	40.066	0.755	58
11	40.306	0.870	61	11	40.317	0.820	61
12	40.505	0.900	63	12	40.513	0.858	63
13	40.668	0.858	65	13	40.674	0.820	65
14	40.790	0.858	66	14	40.794	0.820	66
15	40.887	0.858	67	15	40.890	0.820	67
16	40.965	0.858	68a	16	40.968	0.820	68a
17	41.029	0.858	68c	17	41.031	0.820	68c
∞	41.499	-	-	∞	41.499	-	-

TABLE V. Rydberg series of resonances due to $4s \rightarrow np$ transitions from the $^3P_1$ state of Se^{2+} converging to the $^4P_{3/2}$ series limit in Se^{3+} differentiated by intermediate excited-state fine-structure splitting as identified in the 24 meV photon energy resolution spectrum. Tabulated feature numbers correspond to those identified in Figure 2.

Initial Se^{2+} state: $4s^24p^2$ ($^3P_1$)							
Rydberg Series $4s4p^2(^3P_1)$, $4s \rightarrow np, (^1P_1)$				Rydberg Series $4s4p^2(^3P_1)$, $4s \rightarrow np, (^1S_0)$			
n	Energy (eV)	δ	Feature #	n	Energy (eV)	δ	Feature #
5	34.361	0.858	32	5	34.491	0.820	33
6	36.850	0.868	40	6	36.927	0.825	41
7	38.260	0.852	49	7	38.308	0.805	50
8	39.125	0.818	53	8	39.150	0.780	53
9	39.652	0.858	55	9	39.667	0.820	55
10	40.055	0.790	58	10	40.066	0.755	58
11	40.306	0.870	61	11	40.317	0.820	61
12	40.505	0.900	63	12	40.513	0.858	63
13	40.668	0.858	65	13	40.674	0.820	65
14	40.790	0.858	66	14	40.794	0.820	66
15	40.887	0.858	67	15	40.890	0.820	67
16	40.965	0.858	68a	16	40.968	0.820	68a
17	41.029	0.858	68c	17	41.031	0.820	68c
∞	41.499	-	-	∞	41.499	-	-

with quantum defect theory as applied to Rydberg series resonance identifications: the spectrum restricts the IP to a very narrow energy window where it is low enough to allow the first resonances of the series to be above threshold, but not so low as to allow the next lower resonance to appear (in this case, the next lower resonance would be $n = 14$ for the series in Figure 4). This restricted the IP to a window of approximately ± 40 meV (the average energy window between the $n = 14$ and $n = 15$ resonances of the identified series). Once adjusted, the series identifications progressed normally with only subtle adjustments needed to the IP. A strong indication of the accuracy of the new IP is the diminished oscillator strengths of the first resonances of each instance of the identified series. These first resonances occur so near threshold that the narrow distribution of energies in the photon beam is enough to leave only a portion of the photon flux above the IP. This behavior is consistent in all three occurances of the series where the thresholds fall within their first resonances.

The lone Rydberg resonance series identified in Figure 4 is due to $4p \rightarrow nd$ autoionizing transitions converging to the $^2P_{3/2}$ series limit in Se^{3+} and seen originating from the $^3P_1$, $^3P_2$, and $^1D_2$ metastable states of Se^{2+} ($n_o = 15$ in all three instances), where n_o is the principal quantum number of the first member of the

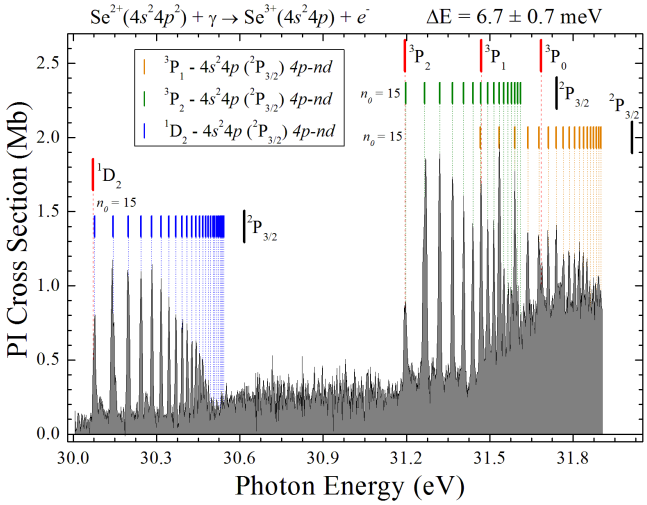

FIG. 4. (Color online) Rydberg series of resonances due to $4p \rightarrow nd$ transitions converging to the $4s^2 4p\ (^2P_{3/2})$ series limit in Se^{3+}. Series limits where $n = \infty$ are indicated by heavy vertical bars with corresponding labels. The ionization thresholds for the $^3P_0$ ground state and $^3P_1$, $^3P_2$, and $^1D_2$ metastable state are indicated by vertical bars with dashed lines [20].

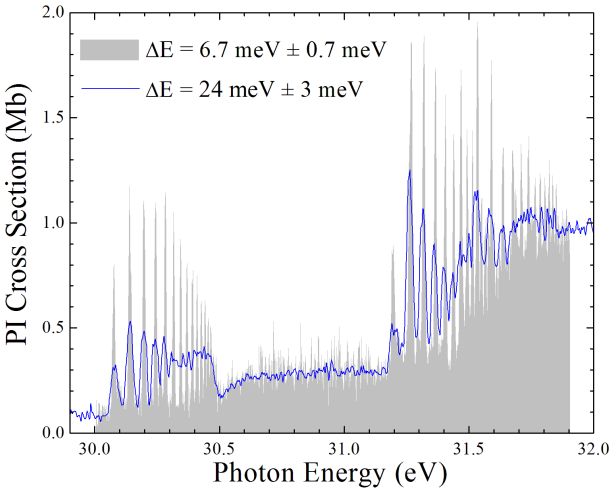

FIG. 5. (Color online) Comparison of the 24 meV (line) and 6.7 meV (solid gray fill) photon energy resolution measurements. The integrated oscillator strength of the low-resolution absolute cross-section measurements was used as a reference to place the high-resolution measurements on an absolute cross-section scale. Note the additional features resolved in the high-resolution measurements which facilitated the precise Rydberg series resonance identifications that were instrumental in the accurate determination of the ionization potential of Se^{2+}.

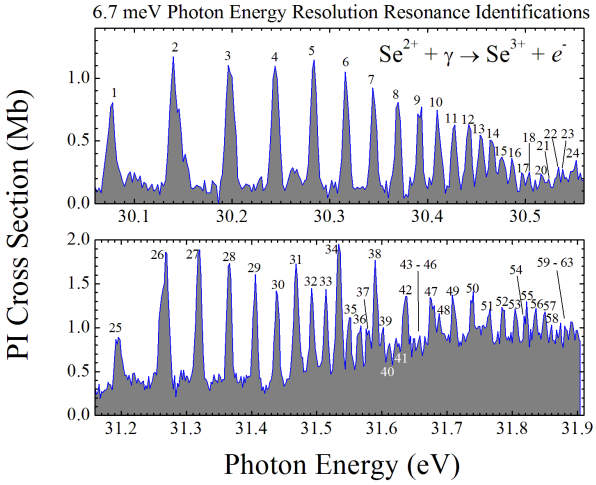

FIG. 6. (Color online) Resonance feature numbering scheme used in the Se^{2+} Rydberg series identification tables associated with the 6.7 meV photon energy resolution spectrum.

Rydberg series detected. The details of this series are listed in Table VI. In support of the series identification, it is expected that the series should not occur from the $^3P_0$ ground state of Se^{2+} as only an excited initial state can support $4p \rightarrow nd$ autoionizing transitions from the $4s^2 4p^2$ ground state configuration. This expectation is verified as the identified series is not seen originating from the $^3P_0$ ground state.

IV. THEORY

A. Fully-relativistic DARC Calculations

The study of the photoabsorption spectrum of trans-Fe elements like selenium and its iso-nuclear sequence is interesting due to the open-shell features of these complexes and the role played by electron correlation effects. In a similar manner to our previous work on singly ionized selenium [18], we carried out large-scale, close-coupling calculations (here we included the lowest 338 levels of the residual Se^{3+} ion in our model) and benchmarked our results with the experimental measurements. The target wavefunctions for our work were obtained using the GRASP code [14, 38, 39], and the subsequent photoionizations cross section calculations were obtained with the DARC codes. All our photoionization cross section calculations were performed within the relativistic Dirac-Coulomb R-matrix approximation [14–16]. An efficient parallel version of the DARC suite of codes has been developed to address the challenge of electron and photon interactions with atomic systems catering for hundreds of levels and thousands of scattering channels.

For comparison with high-resolution measurements

TABLE VI. Rydberg series of resonances due to $4p \rightarrow nd$ transitions from the $^3P_1$, $^3P_2$, and $^1D_2$ excited states of Se^{2+} converging to the $^2P_{3/2}$ series limit in Se^{3+} as identified in the 6.7 meV photon energy resolution spectrum. Tabulated feature numbers correspond to those identified in Figure 6.

Initial Se^{2+} state: $4s^24p^2$												
Rydberg Series $4s^24p$ ($^3P_1$), $4p \rightarrow nd$				Rydberg Series $4s^24p(^3P_2)$, $4p \rightarrow nd$				Rydberg Series $4s^24p(^1D_2)$, $4p \rightarrow nd$			
n	Energy (eV)	δ	Feature #	n	Energy (eV)	δ	Feature #	n	Energy (eV)	δ	Feature #
15	31.466	0.144	31	15	31.198	0.066	25	15	30.077	0.025	1
16	31.534	0.144	34	16	31.265	0.066	26	16	30.143	0.025	2
17	31.590	0.144	38	17	31.320	0.066	27	17	30.198	0.025	3
18	31.637	0.144	42	18	31.366	0.066	28	18	30.244	0.025	4
19	31.677	0.144	47	19	31.405	0.066	29	19	30.283	0.025	5
20	31.710	0.144	49	20	31.439	0.066	30	20	30.316	0.025	6
21	31.739	0.144	50	21	31.468	0.066	31	21	30.345	0.025	7
22	31.765	0.144	51	22	31.492	0.066	32	22	30.369	0.025	8
23	31.787	0.144	52	23	31.514	0.066	33	23	30.391	0.025	9
24	31.806	0.144	53	24	31.533	0.066	34	24	30.410	0.025	10
25	31.823	0.144	55	25	31.550	0.066	35	25	30.427	0.025	11
26	31.838	0.144	56	26	31.565	0.066	36	26	30.442	0.025	12
27	31.851	0.144	57	27	31.578	0.066	37	27	30.455	0.025	13
28	31.863	0.144	58	28	31.590	0.066	38	28	30.467	0.025	14
29	31.874	0.144	60	29	31.601	0.066	39	29	30.477	0.025	15
30	31.884	0.144	61	30	31.610	0.066	40	30	30.487	0.025	16
31	31.892	0.144	62	31				31	30.495	0.025	17
32	31.900	0.144	63	32				32	30.503	0.025	18
33				33				33	30.510	0.025	19
34				34				34	30.517	0.025	20
35				35				35	30.523	0.025	21
36				36				36	30.528	0.025	22
37				37				37	30.533	0.025	22
38				38				38	30.538	0.025	23
39				39				39	30.542	0.025	24
∞	32.021	-	-	∞	31.747	-	-	∞	30.623	-	-

made at the ALS, state-of-the-art theoretical methods used highly correlated wavefunctions that include relativistic effects. Metastable states are populated in the Se^{2+} ion beam experiments and require additional theoretical calculations to be carried out. Recent modifications to the Dirac-Atomic *R*-matrix-Codes (DARC) [16, 18, 19, 40–42] now allow high quality photoionization cross section calculations to be made on heavy complex systems (Fe-peak elements and Mid-Z atoms) of prime interest to astrophysics and plasma applications. Cross-section calculations for various trans-Fe element single photoionization of Se^+ , Xe^+ , Kr^+ , Xe^{7+} [18, 19, 28, 43], $2p^{-1}$ inner-shell studies on Si^+ ions [44], valence-shell studies on neutral Sulfur [45], Tunsgten and its ions [46, 47] have been made using these DARC codes. Suitable agreement of the DARC photoionization cross-sections with high resolution measurements made at leading synchrotron light sources such as ALS, ASTRID, SOLEIL and PETRA III have been obtained.

B. Dirac Coulomb R-matrix

To benchmark theoretical results with the present experimental measurements, photoionization cross sections calculations on this doubly charged ion of seleneium were performed for both the ground and the excited metastable levels associated with the $3d^{10}4s^24p^2$ and $3d^{10}4s4p^3$ configurations. Hibbert and co-workers have shown that two-electron promotions in the target wavefunctions are important to include to get accurate energies, f-values and Einstien coefficients [48, 49] which we include in the present study. In our photoionization cross section calculations for this element, all 338 levels arising from the eighteen configurations: $3d^{10}4s^24p$, $3d^{10}4s4p^2$, $3d^{10}4p^3$, $3d^{10}4s^24d$, $3d^{10}4s4d^2$, $3d^{10}4p4d^2$, $3d^{10}4p^24d$, $3d^{10}4d^3$, $3d^{10}4s4p4d$, $3d^{10}4s^25s$, $3d^{10}4s^25p$, $3d^{10}4s^25d$, $3d^{10}4p^25s$, $3d^{10}4p^25p$, $3d^{10}4p^25d$, $3d^{10}4d^25s$, $3d^{10}4d^25p$, and $3d^{10}4d^25d$, of the residual selenium triply ionized ion (Se^{3+}) are included in the close-coupling collision calculations. Table VII shows the comparison of the energies for the lowest 12 levels of the residual Se^{3+} ion from the 338-level model compared to the available experimental values [20]. As seen from Table VII the theoretical energies obtained from the GRASP code are within a few

percent of the available experimental tabulations. The error quoted is the difference with the NIST tabulations [20].

Photoionization cross section calculations with this 338-level model were performed for the $^3P_0$ ground and metastable $^3P_{1,2}$, $^1D_2$, $^1S_0$ and $^5S^o_2$ states of this trans-Fe element, over the photon energy range of interest. All the cross section calculations were carried out within the Dirac-Coulomb R-matrix approximation [16, 18, 19, 40–42]. The R-matrix boundary radius of 11.52 Bohr radii was sufficient to envelop the radial extent of all the n = 5 atomic orbitals of the residual Se^{3+} ion. A basis of 15 continuum orbitals was sufficient to span the incident experimental photon energy range from threshold up to ∼s 45 eV. This moderate size collision problem involved dealing with around ∼ 2000 coupled channels in the close-coupling calculations with dipole and Hamiltonian matrices of the order of ∼ 30,000 in size. Similarly here for the $4s^24p^2$ ground-state configuration, photoionization out of the $^3P_{2,1,0}$ levels require the bound-free dipole matrices, $J^\pi = 2^e,1^e, 0^e \rightarrow J'^{\pi'} = 0^o,1^o,2^o,3^o$ and for the excited $^1D_2$ and $^1S_0$ metastable states, the bound-free dipole matrices, $J^\pi = 0^e, 2^e \rightarrow$ S $J'^{\pi'} = 1^o, 2^o, 3^o$. We also performed calculations for the additional excited metastable state $4s4p^3\ ^5S^o_2$ where here the $J^\pi = 2^o, \rightarrow J'^{\pi'} = 1^e, 2^e, 3^e$ transitions are required. It was necessary to carry out all these additional photoionization cross-section calculations to span the entire photon energy range (23.5 – 42.5 eV) of the experimental measurements, where various metastable states of this trans-Fe ion are present in the beam.

C. Photoionization

The photoionization cross section calculations were performed in the Dirac Coulomb R-matrix approximation. The efficient suite of parallel DARC codes running on high performance computers (HPC) world-wide, allows one to concurrently form and diagonalise large-scale Hamiltonian and dipole matrices required for electron or photon collisions with atomic systems. This allows large-scale cross-section calculations to be completed in a timely manner. In our calculations for the ground and metastable levels, the outer region electron-ion collision problem was solved with a very fine mesh of 2×10^{-8} Rydbergs (0.272 μeV) so that all the extremely narrow resonance features in the appropriate photoionization cross sections were fully resolved. The jj -coupled Hamiltonian diagonal matrices were adjusted so that the theoretical term energies matched the recommended experimental values of the NIST tabulations [20]. We note that this energy adjustment ensures better positioning of resonances relative to all thresholds included in the present calculations.

TABLE VII. Comparison of the theoretical energies from the GRASP code[14, 38, 39] in the 338-level approximation with the available NIST tabulated values [20]. Relative energies are given in Rydbergs. A sample of the 12 lowest levels for the Se^{3+} (SeIV) ion from the NIST tabulated values are shown compared with the 338 level approximation. The absolute percentage Δ (%) and energy difference between the theoretical values and the tabulated NIST values are included for completeness.

Level	Configuration	Term	NIST Energy[a] (Ry)	GRASP Energy[b] (Ry)	Δ (%) –
1	$4s^24p$	$^2P^o_{1/2}$	0.00000	0.00000	0.0
2	$4s^24p$	$^2P^o_{3/2}$	0.03988	0.03952	-0.9
3	$4s4p^2$	$^4P_{1/2}$	0.72350	0.67551	-7.1
4	$4s4p^2$	$^4P_{3/2}$	0.73795	0.69103	-6.8
5	$4s4p^2$	$^4P_{5/2}$	0.76172	0.71333	-6.9
6	$4s4p^2$	$^2D_{3/2}$	0.94964	0.95985	+1.1
7	$4s4p^2$	$^2D_{5/2}$	0.95415	0.96367	+1.0
8	$4s4p^2$	$^2S_{1/2}$	1.17359	1.21923	+3.7
9	$4s4p^2$	$^2P_{1/2}$	1.24054	1.29735	+4.4
10	$4s4p^2$	$^2P_{3/2}$	1.26077	1.31847	+4.4
11	$4s^24d$	$^2D_{3/2}$	1.39621	1.46294	+4.6
12	$4s^24d$	$^2D_{5/2}$	1.38876	1.46540	+4.5

[a] NIST tabulated values [20].
[b] Theoretical energies from the 338-level approximation.
[c] Δ (%) absolute difference with the NIST values [20].

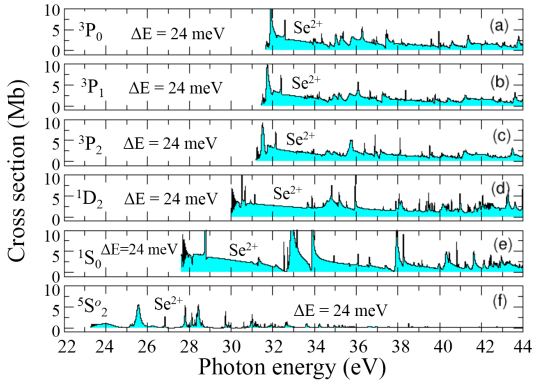

FIG. 7. (Color online) DARC photoionization cross sections results for each of the $4s^24p^2$ ($^3P_{0,1,2}$,$^1D_2$,$^1S_0$) and $4s4p^3$ ($^5S^o_2$) initial states of the Se^{2+} ion, panels (a) – (f), respectively, over the energy range 22 – 42 eV. In panel (f) we have divided the theoretical cross section for the $4s4p^3$ ($^5S^o_2$) initial state by a factor of 20 in order to plot the results on the same scale. The theoretical DARC results shown have been convoluted with a Gaussian having a profile of 24 meV at full width half maximum (FWHM).

TABLE VIII. Theoretical ionization energies (eV) for the $4s^24p^2\ ^3P_{0,1,2},^1D_2,^1S_0$ and the $4s4p^3\ ^5S^o_2$ levels from the closed channels DARC calculations in the 338-level approximation, obtained for the Se^{2+} ion compared with the available NIST tabulated values [20] and an estimate using the Cowan code [36]for the $4s4p^3\ ^5S^o_2$ level . The absolute percentage difference Δ (%) and energy difference (eV) between the theoretical values and the experimental values are included for completeness.

Level	Configuration	Term	Experiment NIST/ALS Energy[a](eV)	Theory Dirac R-matrix (DARC) Energy[b](eV)	Theory/Experiment Δ_1^c Energy (eV)	Δ_2^d (%)
Ground state	$4s^24p^2$	$^3P_0$	31.6965[a]	31.6712[b]	0.0253	0.30
Metastable	$4s^24p^2$	$^3P_1$	31.4806[a]	31.3126[b]	0.0157	0.05
Metastable	$4s^24p^2$	$^3P_2$	31.2084[a]	31.1957[b]	0.0127	0.04
Metastable	$4s^24p^2$	$^1D_2$	30.0808[a]	30.0162[b]	0.0646	0.22
Metastable	$4s^24p^2$	$^1S_0$	28.1716[a]	27.9358[b]	0.2359	0.84
Metastable	$4s4p^3$	$^5S_2$	23.8064[e]	23.8494[f]	0.0430	0.18
				23.6562[b]	0.1503	0.63

[a]NIST tabulated values [20].
[b]DARC closed channel 338-level approximation.
[c]Δ_1 Absolute energy diffference in eV with NIST values.
[d]Δ_2 (%) absolute difference with NIST values and the Cowan code.
[e]Esteves PhD thesis [50], estimated using the Cowan code.
[f]DARC closed channel 40-level approximation.

V. COMPARISON OF THEORY AND EXPERIMENT

Table VIII shows the closed channel bound state DARC calculations for the initial $^3P_0$ ground state, the $^3P_{1,2}$, $^1D_2$, $^1S_0$ and $^5S^o_2$ metastable states of this trans-Fe element. A similar comparison with the available values from the NIST tabulations [20] is given. We note no value exists for the $4s4p^3\ ^5S^o_2$ ionization potential in the NIST tabulations [20]. An estimate was made for it using the Cowan code [36] and from closed channel DARC calculations. From Table VIII we see that the value obtained from the Cowan codes is in suitable accord (within 150 meV) of the value obtained from the close-channel DARC calculations. Furthermore, for the remaining bound states (ionization potentials) investigated here we see that the results from the DARC large-scale closed channel calculations deviate from the tabulated NIST ionization potentials [20] by values ranging from 12 meV – 236 meV and illustrates the difficulty of treating electron correlation in open-shell complex ions accurately.

Figure 7 illustrates the large-scale DARC photoionization cross section calculations for each of the initial $^3P_0$ ground state, the $^3P_{1,2}$, $^1D_2$, $^1S_0$ and $^5S^o_2$ metastable states of the Se^{2+} ion. The theoretical cross sections have been shifted to match the experimental ionization potentials given in Table VIII. The theoretical photoionization cross sections from the DARC calculations have been convoluted with a Gaussian having a profile width of 24 meV in order to simulate the experimental results from the Advanced Light Source.

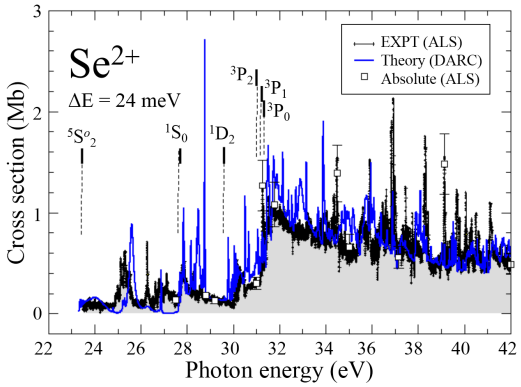

FIG. 8. (Color online) Comparison of the DARC photoionization cross sections results obtained for each of the $4s^24p^2$ ($^3P_{0,1,2},^1D_2,^1S_0$) and $4s4p^3$ ($^5S^o_2$) initial states of the Se^{2+} ion with the ALS experimental results. To simulate the ALS experiment the theoretical DARC results have been convoluted with a Gaussian having a profile width of 24 meV and an appropriate admixture of the population intensity used to best suit the high resolution ALS experimental data. See text for details.

Finally, to simulate experiment the theoretical photoionization cross sections for each initial state was convoluted at the experimental resolution of 24 meV and a suitable admixture of the initial states present in the beam carried out. We have normalised theory to the high resolution absolute experimental cross sections which al-

lows for a more meaningful comparison to be made from which one can make an estimate of the error in the theoretical work.

In Figure 8 we present a comparison between theory and experiment for the photon energy range 23.5 - 42.5 eV. We find that an admixture of the intensity population; 1% $^5S^o_2$, 5%$^1S_0$, 10%$^1D_2$, with the remaining 84 % distributed among the $^3P_{2,1,0}$ levels (47% $^3P_2$, 28% $^3P_1$ and 9% $^3P_0$) appears to gives satisfactory agreement with experiment. This also reproduces the main features in the experimental spectra.

An additional check on the theoretical data is a comparison of the integrated oscillator strength f with experiment. The integrated oscillator strength f of the experimental spectra was calculated using [51],

$$f = 9.1075 \times 10^{-3} \int \sigma(h\nu) dh\nu \qquad (2)$$

and yielded a value of 0.087 ± 0.017 from the present ALS measurements.

A similar procedure for the theoretical R- matrix cross-section (from appropriated weighted initial states) gave a value of 0.096568 again in respectable agreement with experiment. This allows one to quantify an error estimate which we conservatively give as 10% in our theoretical cross sections.

VI. CONCLUSIONS

We have presented absolute single photoionization cross-section measurements for Se^{2+} from the low-lying metastable state ionization region to above the ground state ionization threshold at a photon energy resolution of 24 ± 3 meV. Initial analysis indicated a discrepancy between the reported and measured ionization potential which motivated additional, high-resolution measurements in the energy region of the ground state threshold. These measurements, from 30.0 eV to 31.9 eV, were conducted at an energy resolution of 6.7 ± 0.7 meV. The analysis of the Rydberg series of resonances in the high resolution spectrum necessitated a shift in the historically reported ionization potential of Se^{2+} of 0.843 ± 0.018 eV. A similar shift was independently reported by another research group which is in agreement with the present results and within the energy uncertainties of both experimental studies [52].

Three distinct Rydberg resonance series have been found and identified in the spectra of this trans-Fe ion. One series of the form $4s \rightarrow np$ is identified originating from the $^3P_2$ and $^1D_2$ metastable states and converging to the $^2D_{5/2}$ series limit in Se^{3+}. A second $4s \rightarrow np$ series is identified originating from the $^3P_1$ metastable state but converging to the $^4P_{3/2}$ series limit in Se^{3+} in which fine structure splitting was observed and resolved. Finally, a Rydberg series of the form $4p \rightarrow nd$ and originating from the $^3P_1$, $^3P_2$ and $^1D_2$ metastable states was found converging to the $^2P_{3/2}$ series limit in Se^{3+}. Resonances energies and quantum defects for these series have been tabulated in Tables IV, V, and VI for completeness.

Large-scale DARC calculations have been performed for the $4s^24p^2$ ($^3P_{0,1,2}$,$^1D_2$,$^1S_0$) and $4s4p^3$ ($^5S^o_2$) initial states. The theoretical results, when convoluted with a Gaussian having a 24 meV profile and an appropriate admixture of the population intensities, show suitable agreement with the ALS experimental results and reproduces the main features in the spectra. Larger target representations in the close-coupling DARC photoionization cross section calculations would naturally provide more accurate results for resonance positions and total cross sections. However, we have access to only a finite amount of computational resources and the present results provide a satisfactory attempt at simulating the high-resolution ALS experimental measurements. Extended photoionization cross section calculations on this open-shell complex ion would also be desirable.

The high resolution experimental measurements made at the ALS synchrotron radiation facility (over a limited energy range) have been used to benchmark theoretical calculations which would be suitable to be incorporated into astrophysical modelling codes like Cloudy [53, 54], XSTAR [55] and AtomDB [56] used to numerically simulate the thermal and ionization structure of ionized astrophysical nebulae.

ACKNOWLEDGMENTS

Support by the Office of Science, Office of Basic Energy Sciences, of the U.S. Department of Energy under contracts DE-AC02-05CH11231, DE-AC03-76SF-00098, and grant DE-FG02-03ER15424 is gratefully acknowledged. D. M. acknowledges support from the Doctoral Fellowship in Residence Program at the Advanced Light Source and the Montana Space Grant Consortium. N. C. S. acknowledges support from an NSF Astronomy and Astrophysics Postdoctoral Fellowship under award AST-0901432 and from NASA grant 06-APRA206-0049. B. M. M. acknowledges support by the US National Science Foundation under the visitors program and through a grant to ITAMP at the Harvard-Smithsonian Center for Astrophysics, Queen's University Belfast through a visiting research fellowship (VRF). This research used resources of the National Energy Research Scientific Computing Center, which is supported by the Office of Science of the U.S. Department of Energy (DOE) under Contract No. DE-AC02-05CH11231. The computational work was performed at the National Energy Research Scientific Computing Center in Oakland, CA, USA and at The High Performance Computing Center Stuttgart (HLRS) of the University of Stuttgart, Stuttgart, Germany. This research also used resources of the Oak Ridge Leadership Computing Facility at the Oak Ridge National Laboratory, which is supported by the Office of Science of the U.S. Department of Energy (DoE) under Contract No.

DE-AC05-00OR22725.

[1] I. U. Roederer, Astrophys. J. **756**, 36 (2012).

[2] I. U. Roederer, J. J. Cowan, G. W. Preston, S. A. Shechtman, C. Sneden, and I. B. Thompson, Mon. Not. Roy. Astron. Soc. **445**, 2970 (2012).

[3] N. C. Sterling and H. L. Dinerstein, Astrophys. J. Suppl. Ser. **174**, 158 (2008).

[4] R. D. Blum and P. J. McGregor, Astron. J **135**, 1708 (2008).

[5] J. Garcia-Rojas, S. Madona, V. Luridana, N. C. Sterling, C. Morisset, G. Delgado-Inglada, and L. T. S. Cipriano, Mon. Not. Roy. Astron. Soc **452**, 2606 (2015).

[6] N. C. Sterling, H. L. Dinerstein, and T. R. Kallman, Astrophys. J. Suppl. Ser. **169**, 37 (2007).

[7] N. C. Sterling, R. L. Porter, and H. L. Dinerstein, Astrophys. J. Suppl. Ser. **218**, 25 (2015).

[8] N. C. Sterling, M. C. Witthoeft, D. A. Esteves, R. C. Bilodeau, A. L. D. Kilcoyne, E. C. Red, R. A. Phaneuf, G. A. Alna'Washi, and A. Aguilar, Can. J. Phys. **89**, 379 (2011).

[9] N. C. Sterling, D. A. Esteves, R. C. Bilodeau, A. L. D. Kilcoyne, E. C. Red, R. A. Phaneuf, and A. Aguilar, J. Phys. B: At. Mol. Opt. Phys. **44**, 025701 (2011).

[10] D. A. Esteves, R. C. Bilodeau, N. C. Sterling, R. A. Phaneuf, A. L. D. Kilcoyne, E. C. Red, and A. Aguilar, Phys. Rev. A. **84**, 013406 (2011).

[11] D. A. Esteves, R. C. Bilodeau, R. A. Phaneuf, A. L. D. Kilcoyne, E. C. Red, and A. Aguilar, J. Phys. B: At. Mol. Opt. Phys. **45**, 115201 (2012).

[12] N. C. Sterling, Astron. Astrophys. **533**, A62 (2011).

[13] N. C. Sterling and M. C. Witthoeft, Astron. Astrophys. **529**, A147 (2011).

[14] I. P. Grant, *Quantum Theory of Atoms and Molecules: Theory and Computation* (Springer, New York, USA, 2007).

[15] P. G. Burke, *R-Matrix Theory of Atomic Collisions: Application to Atomic, Molecular and Optical Processes* (Springer, New York, USA, 2011).

[16] DARC codes URL, `http://connorb.freeshell.org`.

[17] V. Fivet, M. Bautista, and C. Ballance, J. Phys. B: At. Mol. Opt. Phys. **45**, 035201 (2012).

[18] B. M. McLaughlin and C. P. Ballance, J. Phys. B: At. Mol. Opt. Phys. **45**, 095202 (2012).

[19] B. M. McLaughlin and C. P. Ballance, J. Phys. B: At. Mol. Opt. Phys. **45**, 085701 (2012).

[20] Y. Ralchenko, A. E. Kramida, J. Reader, and N. A. Team, "Nist atomic spectra database (version 5.2)," National Institute of Standards and Technology, Gaithersburg, MD, USA (2014).

[21] A. M. Covington, A. Aguilar, I. R. Covington, M. F. Gharaibeh, C. A. Shirley, R. A. Phaneuf, I. Álvarez, C. Cisneros, G. Hinojosa, J. D. Bozek, I. Dominguez, M. M. Sant'Anna, A. S. Schlachter, N. Berrah, S. N. Nahar, and B. M. McLaughlin, Phys. Rev. Lett. **87**, 243002 (2001).

[22] A. M. Covington, A. Aguilar, I. R. Covington, M. F. Gharaibeh, G. Hinojosa, C. A. Shirley, R. A. Phaneuf, I. Álvarez, C. Cisneros, I. Dominguez-Lopez, M. M. Sant'Anna, A. S. Schlachter, B. M. McLaughlin, and A. Dalgarno, Phys. Rev. A **66**, 062710 (2002).

[23] G. A. Alna'washi, M. Lu, M. Habibi, R. A. Phaneuf, A. L. D. Kilcoyne, A. S. Schlachter, C. Cisneros, and B. M. McLaughlin, Phys. Rev. A **81**, 053416 (2010).

[24] M. Habibi, D. Esteves, R. A. Phaneuf, A. L. D. Kilcoyne, A. Aguilar, and C. Cisneros, Phys. Rev. A **80**, 033407 (2009).

[25] M. Gharaibeh, A. Aguilar, A. M. Covington, E. D. Emmons, S. W. J. Scully, R. A. Phaneuf, and A. Müller, Phys. Rev. A **83**, 043412 (2011).

[26] A. M. Covington, A. Aguilar, I. R. Covington, G. Hinojosa, C. A. Shirley, R. A. Phaneuf, I. Álvarez, C. Cisneros, I. Dominguez-Lopez, M. M. Sant'Anna, A. S. Schlachter, C. P. Ballance, and B. M. McLaughlin, Phys. Rev. A **84**, 013413 (2011).

[27] J. M. Bizau, C. Blancard, M. Coreno, D. Cubaynes, C. Dehon, N. E. Hassan, F. Folkmann, M. F. Gharaibeh, A. Giuliani, J. Lemaire, A. R. Milosavljevi, C. Nicolas, and R. Thissen, J. Phys. B: At. Mol. Opt. Phys. **44**, 055205 (2011).

[28] A. Müller, S. Schippers, D. Esteves-Macaluso, M. Habibi, A. Aguilar, A. L. D. Kilcoyne, R. A. Phaneuf, C. P. Ballance, and B. M. McLaughlin, J. Phys. B: At. Mol. Opt. Phys. **47**, 215202 (2014).

[29] E. M. Hernández, A. M. Juárez, A. L. D. Kilcoyne, A. Aguilar, L. Hernández, A. Antillón, D. Macaluso, A. Morales-Mori, O. González-Magaña, D. Hanstrop, A. M. Covington, V. Davis, D. Calabrese, and G. Hinojosa, J. Quant. Spec. Rad. Trans. **151**, 217 (2015).

[30] I. C. Lyons, B. Pert, J. B. West, and K. Dolder, J. Phys. B: At. Mol. Phys. **19**, 4137 (1986).

[31] F. Broetz, R. Trassl, R. W. McCullough, W. Arnold, and E. Salzborn, Phys. Scr. **92**, 278 (2001).

[32] R. Trassl, W. R. Thompson, F. Broetz, M. Pawlowsky, R. W. McCullough, and E. Salzborn, Phys. Scr. **80**, 504 (1999).

[33] K. Rinn, A. Müller, H. Eichenaue, and E. Salzborn, Rev. Sci. Instrum. **53**, 829 (1982).

[34] D. Attwood, *Soft X-rays and Extreme Ultraviolet Radiation* (Cambridge University Press, New York, 1999).

[35] M. Domke, K. Schulz, G. Remmers, G. Kaindl, and D. Wintgen, Phys. Rev. A **53**, 1424 (1996).

[36] R. D. Cowan, *The Theory of Atomic Structure and Spectra* (University of California Press, Berkeley, California, USA, 1981).

[37] M. J. Seaton, Rep. Prog. Phys. **46**, 167 (1983).

[38] K. G. Dyall, I. P. Grant, C. T. Johnson, and E. P. Plummer, Comput. Phys. Commun. **55**, 425 (1989).

[39] F. Parpia, C. F. Fischer, and I. P. Grant, Comput. Phys. Commun. **94**, 249 (2006).

[40] C. P. Ballance and D. C. Griffin, J. Phys. B: At. Mol. Opt. Phys. **39**, 3617 (2006).

[41] B. M. McLaughlin and C. P. Ballance, in *Sustained Simulated Performance 2014*, edited by M. M. Resch, Y. Kovalenko, E. Fotch, W. Bez, and H. Kobaysah (Springer, Berlin, Germany, 2014) pp. 173–190.

[42] B. M. McLaughlin, C. P. Ballance, M. S. Pindzola, and A. Müller, in *High Performance Computing in Science*

and Engineering'14, edited by W. E. Nagel, D. H. Kröner, and M. M. Resch (Springer, Berlin,Germany, 2014) pp. 23–40.

[43] G. Hinojosa, A. M. Covington, G. A. Alna'Washi, M. Lu, R. A. Phaneuf, I. Álvarez, M. M. Sant'anna, C. Cisneros, I. Álvarez, A. Aguilar, A. L. D. Kilcoyne, A. S. Schlachter, C. P. Ballance, and B. M. McLaughlin, Phys. Rev. A **86**, 063402 (2012).

[44] E. T. Kennedy, J.-P. Mosnier, P. V. Kampen, D. Cubaynes, S. Guilbaud, C. Blancard, B. M. McLaughlin, and J.-M. Bizau, Phys. Rev. A **90**, 063409 (2014).

[45] M. Barthel, R. Flesch, E. Rühl, and B. M. McLaughlin, Phys. Rev. A **91**, 013406 (2015).

[46] C. P. Ballance and B. M. McLaughlin, J. Phys. B: At. Mol. Opt. Phys. **48**, 085201 (2015).

[47] A. Müller, S. Schippers, J. Hellhund, K. Holste, A. L. D. Kilcoyne, R. A. Phaneuf, C. P. Ballance, and B. M. McLaughlin, J. Phys. B: At. Mol. Opt. Phys. **48**, 235203 (2015).

[48] P. Ohja and A. Hibbert, J. Phys. B: At. Mol. Opt. Phys. **22**, 1153 (1987).

[49] F. P. Keenan, P. Ohja, and A. Hibbert, Phys. Scr. **48**, 129 (1993).

[50] D. A. Esteves, "Photoionization of se ions for the determination of elemental abundances in astrophysical nebulae," Thesis (Ph. D.); Publication Number: AAI3404727, University of Reno, Nevada, USA (2010).

[51] U. Fano and J. W. Cooper, Rev. Mod. Phys. **40**, 441 (1968).

[52] A. Tauheed and Hala, Phys. Scr. **85**, 025304 (2012).

[53] G. Ferland, K. T. Korista, D. A. Verner, J. W. Ferguson, J. B. Kingdon, and E. M. Verner, Pub. Astron. Soc. Pac. (*PASP*) **110**, 761 (1998).

[54] G. J. Ferland, Ann. Rev. of Astron. Astrophys. **41**, 517 (2003).

[55] T. R. Kallman, Astrophys. J. Suppl. Ser. **134**, 139 (2001).

[56] A. R. Foster, L. Ji, R. K. Smith, and N. S. Brickhouse, Astrophys. J **756**, 128 (2012).